TRANSACTIONS OF THE ROYAL SOCIETY OF TROPICAL MEDICINE AND HYGIENE (1998) 92, 12–20

Predicting malaria seasons in Kenya using multitemporal meteorological satellite sensor data

Simon I. Hay[1], Robert W. Snow[2,3] and David J. Rogers[1] *[1]Trypanosomiasis and Land-use in Africa (TALA) Research Group, Department of Zoology, University of Oxford, South Parks Road, Oxford, OX1 3PS, UK*; [2]Kenya Medical Research Institute/Wellcome Trust Collaborative Programme, P.O. Box 43640, Nairobi, Kenya; [3]Nuffield Department of Clinical Medicine, University of Oxford, John Radcliffe Hospital, Headington, Oxford, OX3 9DS, UK*

Abstract

This article describes research that predicts the seasonality of malaria in Kenya using remotely sensed images from satellite sensors. The predictions were made using relationships established between long-term data on paediatric severe malaria admissions and simultaneously collected data from the Advanced Very High Resolution Radiometer (AVHRR) on the National Oceanic and Atmospheric Administrations (NOAA) polar-orbiting meteorological satellites and the High Resolution Radiometer (HRR) on the European Organization for the Exploitation of Meteorological Satellites' (EUMETSAT) geostationary Meteosat satellites. The remotely sensed data were processed to provide surrogate information on land surface temperature, reflectance in the middle infra-red, rainfall, and the normalized difference vegetation index (NDVI). These variables were then subjected to temporal Fourier processing and the fitted Fourier data were compared with the mean percentage of total annual malaria admissions recorded in each month. The NDVI in the preceding month correlated most significantly and consistently with malaria presentations across the 3 sites (mean adjusted r^2=0·71, range 0·61–0·79). Regression analyses showed that an NDVI threshold of 0·35–0·40 was required for more than 5% of the annual malaria cases to be presented in a given month. These thresholds were then extrapolated spatially with the temporal Fourier-processed NDVI data to define the number of months, in which malaria admissions could be expected across Kenya in an average year, at an 8 × 8 km resolution. The resulting maps were compared with the only existing map (Butler's) of malaria transmission periods for Kenya, compiled from expert opinion. Conclusions are drawn on the appropriateness of remote sensing techniques for compiling national strategies for malaria intervention.

Keywords: malaria, *Plasmodium falciparum*, seasonality, prediction, satellite data, remote sensing, Kenya

Introduction

It has long been established that the dynamics of disease vector behaviour, abundance and distribution are sensitive to changes in climate. For the mosquito vectors of *Plasmodium falciparum*, these studies arise from entomological observations both across diverse ecological settings and in controlled laboratory investigations (MUIR, 1988). Whilst such investigations have defined climatic ranges which sustain vector life cycles sufficient for parasite development and transmission to human hosts, far fewer studies have examined the ecological variation within these ranges that support the diverse spectrum of seasonal vector activity and disease distribution common to sub-saharan Africa.

Seasonal fluctuations in the basic reproduction rate (BRR) of infection (DIETZ, 1988) occur in nearly every endemic malaria setting. The absence of empirical models relating the BRR to disease outcome, however, makes it unclear how these seasonal changes relate to patterns of malaria morbidity and mortality. Nevertheless, seasonality is a widely accepted feature of clinical malaria in Africa. The malaria burden can range from being concentrated into a few months of the year, as in large areas of West Africa (GAZIN *et al.*, 1988; BREWSTER & GREENWOOD, 1993; BINKA *et al.*, 1994; BOUVIER *et al.*, 1997), through intermediary stages where disease incidence varies annually, such as on the Kenyan coast (SNOW *et al.*, 1993), to areas of perennial transmission with little within-year variation, characteristic of the river valley and lake regions of East Africa (SMITH *et al.*, 1993; SLUTSKER *et al.*, 1994).

There are academic and pragmatic needs for descriptions of the clinical and epidemiological patterns of *P. falciparum*, to guide and rationalize disease control (SNOW *et al.*, 1996). For example, the timing and frequency of insecticide treatment of bed nets or mass drug administration would best be determined by the periods of maximal disease incidence within a community. This has proved successful in streamlining resources in The Gambia, where a change from annual to seasonal targeted chemoprophylaxis was adopted after elucidating the basic epidemiological features of disease in the country (GREENWOOD & PICKERING, 1993). Furthermore, the clinical management of febrile events may also be guided by an understanding of the changing risks of fever due to malaria throughout the year (GREENWOOD *et al.*, 1987).

There has been recent interest in the use of remotely sensed imagery from satellite sensors at a variety of spectral, spatial, and temporal resolutions for mapping the meteorological and other ecological determinants of arthropod disease vector distributions (reviewed by HAY *et al.*, 1997). Previous applications of remote sensing techniques in malaria epidemiology have used both aerial and space-borne sensors to map mosquito larval habitat (WAGNER *et al.*, 1979; LINTHICUM *et al.*, 1987; WOOD *et al.*, 1992; POPE *et al.*, 1994) and to predict adult mosquito abundance (REJMANKOVA *et al.*, 1995; ROBERTS *et al.*, 1996; THOMSON *et al.*, 1996), as well as to estimate malaria risk in specific villages (BECK *et al.*, 1994, 1997). In this paper we extend these techniques to a comparative analysis of remotely sensed climatic and vegetation variables with epidemiological patterns of clinical malaria common to sub-saharan Africa. It is demonstrated how these descriptions can be used to provide a high temporal resolution map of the seasonality of clinical disease throughout a country, using Kenya as an example.

Materials and Methods

Study communities and clinical surveillance of paediatric malaria

The recent description of severe malaria morbidity in 5 communities in Africa by SNOW *et al.* (1997) allowed the detailed examination of short-term temporal fluctuations in malaria morbidity. In brief, these communities were selected on the basis of their close proximity to inpatient hospital facilities with continuing clinical research programmes on severe, life-threatening malaria.

Address for correspondence: Dr S. I. Hay, TALA Research Group, Department of Zoology, University of Oxford, South Parks Road, Oxford, OX1 3PS, UK; phone +44 (0)1865 271257, fax +44 (0)1865 271240, e-mail simon.hay@zoo.ox.ac.uk
*URL address http://users.ox.ac.uk~zoo10120

Table 1. Spatial, temporal and spectral resolution of the sensors carried by the NOAA-11 and Meteosat-5 satellites

Satellite/Sensor	Spectral (μm)[a]	Resolution Spatial (km)	Temporal (h)
National Oceanic and Atmospheric Administration (NOAA)/Advanced Very High Resolution Radiometer (AVHRR)	1 0·58–0·68 2 0·72–1·10 3 3·55–3·93 4 10·30–11·30 5 10·50–11·50	1·1[d]	12
Meteosat/High Resolution Radiometer (HRR)	1 0·40–1·10 2 10·50–12·50 3 5·70–7·10	2·5 5[d] 5	0·5

[a]0·4μm is at the visible end, and 12μm at the thermal end, of the electromagnetic spectrum.
[b]Diameter of the viewing area of the sensor at nadir (i.e., directly below the satellite).
[c]Time taken for the satellite to repeat a measurement over the same Earth location.
[d]By the time the PAL and FAO-CCD data have been processed and distributed they are at 8 × 8 and 7·6 × 7·6 km resolution, respectively.

The Kenyan sites (Kilifi North, Kilifi South and Siaya) were chosen for this investigation (Fig. 4, A).

The communities of Kilifi North and Kilifi South are situated on Kenya's coastline and experience a pronounced bimodal pattern of annual rainfall with a long rainy period between April and July and a shorter one between September and October. The average annual precipitation during the period of disease surveillance was 1071 mm and 1155 mm for Kilifi North and South respectively. A creek separates the communities and the area to the south differs from the north as it is traversed by perennial and seasonal rivers. The rural community of Siaya is 20 km from the shore of Lake Victoria at an altitude of 1130 m. Rainfall occurs in every month of the year, with peaks between March and May and between August and November. The average annual rainfall for the period of study was 1337 mm, similar to that at the Kilifi sites.

Admissions to the paediatric wards of the local hospitals from each community were monitored for between 3 and 5 years. Every admitted patient between one month and 10 years of age was examined by a study physician or clinical officer and details of the clinical histories, observations and the results of laboratory procedures were recorded on a standard proforma. A primary diagnosis for admission was recorded on discharge, following a review of all laboratory and additional clinical investigations. Malaria as the primary cause of admission was defined following the detection of *P. falciparum* infection in the peripheral blood and a review of all supporting haematological, clinical, radiological and microbiological information to exclude other potential causes for the clinical presentation.

NOAA–AVHRR data

The Pathfinder Advanced Very High Resolution Radiometer (AVHRR) Land (PAL) data were obtained for a period of 5 years (1990–1994) coincident with the paediatric malaria admission records. They were derived from the visible and infra-red radiance imagery collected by the AVHRR on board the National Oceanic and Atmospheric Administration's NOAA-11 satellite. A detailed guide to the NOAA meteorological satelites and their AVHRR payload has been given by KIDWELL (1995) and CRACKNELL (1997); the relevant details are summarized in Table 1. A review of the processing techniques used to calibrate, navigate and quality-control images from this AVHRR archive, and a definitive description of the resulting PAL data products, has been given by JAMES & KALLURI (1994).

The PAL data were provided as digital files of daily global coverage containing the 5 channels of AVHRR data and 7 bands of ancillary information. The 5 channels of raw waveband data were extracted for Africa and scaled with information provided by AGBU & JAMES (1994) using Earth Resources Data Analysis System (ERDAS) Imagine 8·2™ on a Silicon Graphics Indy R5000™ workstation. The ancillary information provided with the PAL data was then used to exclude unreliable picture elements (pixels) from the images. Firstly, cloudy pixels, as determined by the 'Clouds from AVHRR' (CLAVR) algorithm (STOWE *et al.*, 1991), were masked. Secondly, pixels viewed by the AVHRR sensor at an angle greater than 42° were eliminated to reduce view angle distortion. Thirdly, those pixels recorded at solar zenith angles greater than 80° were excluded, because at these angles the twilight of dawn or dusk affects measurements. Further information on the factors affecting the quality of remotely sensed data and the techniques often used to ameliorate such problems have been discussed by HAY *et al.* (1996).

These quality-controlled raw waveband data were then processed to provide ecologically meaningful information. The normalized difference vegetation index (NDVI) was first calculated. It is defined for the AVHRR as follows:

$$\mathrm{NDVI} = \frac{(\text{channel 2}-\text{channel 1})}{(\text{channel 2}+\text{channel 1})} \quad (1)$$

with possible values ranging from −1 to +1, but in practice lying well within these limits (TUCKER, 1979). The NDVI, which has no units since it is a ratio, exploits the fact that chlorophyll and carotenoid pigments in plant tissues absorb light in the visible red wavelengths (which corresponds to AVHRR channel 1) whilst mesophyll tissue reflects light in the near infra-red (which corresponds to AVHRR channel 2) (SELLERS, 1985; TUCKER & SELLERS, 1986). Actively photosynthesizing vegetation therefore appears darker in the visible and brighter in the infra-red region than senescent vegetation or the soil background. The NDVI is theoretically a specific measure of chlorophyll abundance and energy absorption (MYNENI *et al.*, 1995), but its use has been extended through multitemporal observations to measure vegetation biomass (TUCKER *et al.*, 1985b) and to classify vegetation type (TUCKER *et al.*, 1985a) and phenology (JUSTICE *et al.*, 1985) in a range of ecosystems throughout Africa.

Land surface temperature (LST) estimates were calculated from simultaneously collected brightness temperatures (K) from AVHRR channels 4 and 5 using an equation derived by PRICE (1984):

$$T = \text{channel 4} + 3{\cdot}33\,(\text{channel 5}-\text{channel 4}). \quad (2)$$

The 3·33 term is a value determined empirically for the NOAA-7 satellite. This relationship holds because signal attenuation is much greater in channel 5 than in channel 4, so the difference between the channels can be used to estimate, and hence correct for, the amount of atmospheric water vapour attenuation. This equation has been demonstrated to provide LST estimates accu-

rate to ± 2–3 K (COOPER & ASRAR, 1989; SUGITA & BRUTASAERT, 1993).

The middle infra-red (MIR) radiance data from AVHRR channel 3 were also processed. Despite being less well documented than other wavebands, MIR wavelengths appear to suffer less atmospheric attentuation than the visible and near infra-red wavelengths (KERBER & SCHUTT, 1986), making these data potentially very suitable for monitoring vegetation in the tropics. Furthermore, MIR has been shown to be more highly correlated with various biophysical properties of vegetation canopies than the visible or near infra-red wavelengths (BOYD *et al.*, 1996). BOYD & CURRAN (in press) provide an exhaustive review of the proposed mechanisms governing the interaction of MIR and vegetated land surface.

Maximum value compositing

The daily acquisition of NOAA–AVHRR data enables sensor data of improved quality to be obtained by combining images over time. The aim of this compositing procedure is to select the most cloud-free and least atmospherically contaminated value for a pixel within the chosen period. Most compositing relies on the fact that the NDVI is reduced by cloud and other atmospheric contamination so that the highest NDVI during a decadal (i.e. 10 d) or monthly period occurs when atmospheric attenuation, and thus data noise, are least (HOLBEN, 1986). This method of image production is called maximum value compositing (MVC). The daily NDVI, LST and MIR data were all subject to MVC over monthly periods. The LST and MIR data were composited using their respective maxima, however, because these values are the least cloud-contaminated in the series, since clouds are generally colder than the land and vegetation at tropical latitudes (LAMBIN & EHRLICH, 1995).

Meteosat–HRR data

The Meteosat–High Resolution Radiometer (HRR) data were supplied by the African Real Time Environmental Monitoring Information System (ARTEMIS) programme of the United Nations (UN) Food and Agriculture Organization (FAO) as processed monthly cold cloud duration (CCD) images from 1990–1994. A guide to the Meteosat satellite series and their HRR payload has been published (ANONYMOUS, 1994) and details of their spatial, spectral and temporal resolution are given in Table 1. The relationship between cloud-top temperature (recorded by channel 2 of the Meteosat satellite) and the probability of rainfall has been established by SNIJDERS (1991). The particular threshold temperature associated with rain-bearing clouds, and the quantity of rain they deposit, vary temporally and spatially however, so must be established empirically. This has been done for large parts of Africa by the Tropical Applications in Meteorology of Satellite and Other Data (TAMSAT) programme (DUGDALE *et al.*, 1995). Kenya lies outside this region, where simple seasonally adjusted thresholds are applied. Africa-wide analyses, however, have shown that CCD–rainfall correlations in these zones are equally robust (HAY, 1996). These results were used by the FAO–ARTEMIS project to generate monthly CCD images, where each pixel represents the number of hours during which there was cloud cover colder than the threshold value for the compositing period.

Temporal Fourier analysis

The 5 years series of monthly NDVI, LST, MIR and CCD images were then subjected to temporal Fourier analysis, since this technique has been demonstrated to achieve significant data reduction of remotely sensed time series without a commensurate loss of biological information (ROGERS & WILLIAMS, 1994). The analysis decomposes seasonal changes in the satellite-sensor variables into the sum of their sinusoidal components with frequencies of one up to 6 cycles per year, so that the first term in the Fourier expansion gives the annual cycle, the second the biannual cycle, and so on (ROGERS *et al.*, 1996). The sum of the different components then describes the observed annual variation at the site in question. The first 3 Fourier terms capture most of the variation in the signal, and only these were used in the present study. The analysis also gives information on both the phase (timing in the year of maximum value) and amplitude (maximum range around the mean annual value) of each component and these were used to construct the fitted signal, from which may be extracted the number of months above or below any threshold value.

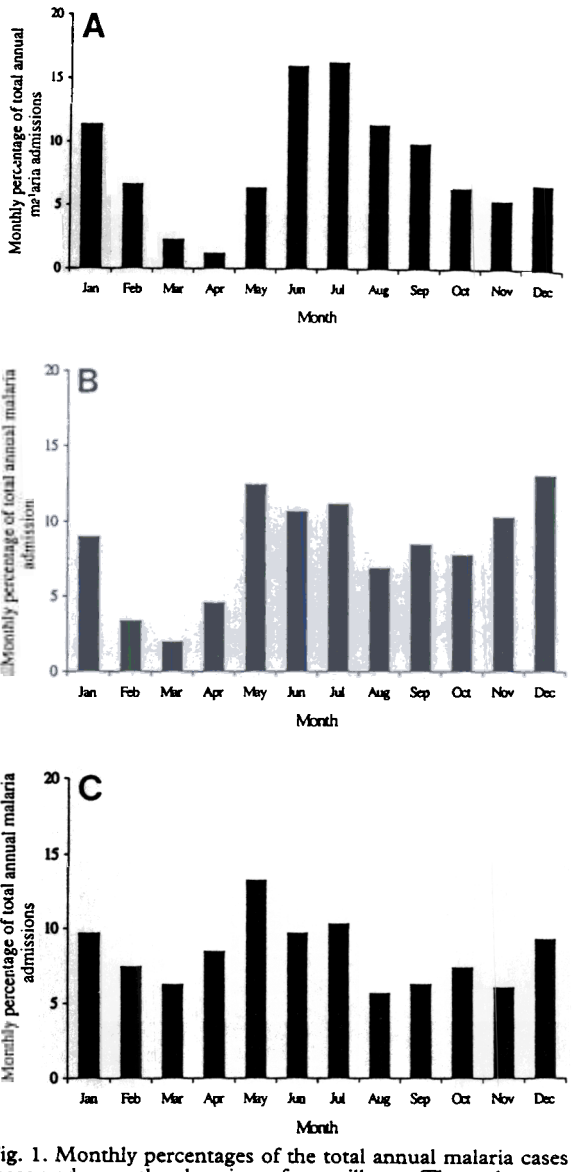

Fig. 1. Monthly percentages of the total annual malaria cases measured over the duration of surveillance. These data are therefore the average annual pattern of admissions shown for (A) Kilifi North, (B) Kilifi South and (C) Siaya.

Data analysis and malaria seasonality prediction

The latitude and longitude of each hospital were used to extract values from the Fourier-processed satellite sensor data. A mean value was taken from a 3 × 3 pixel array around the centre pixel (corresponding to an area of approximately 24 × 24 km), since this area encompassed the whole of the community in each of the study

Table 2. Adjusted coefficients of determination (adjusted r^2) relating the mean monthly temporal Fourier-processed satellite sensor variables and mean monthly percentage of annual malaria admissions for the three study sites

Sensor variable[b]	Lag[c] (months)	Adjusted r^2[a] Kilifi North	Kilifi South	Siaya
MIR	0	−0·38*	−0·48*	−0·14
	−1	−0·67**	−0·38*	−0·09
	−2	−0·27	−0·03	−0·04
LST	0	−0·46*	−0·41*	−0·15
	−1	−0·64**	−0·29	−0·05
	−2	−0·20	−0·03	0·07
NDVI	0	0·06	0·55**	0·28
	−1	0·79**	0·74**	0·61**
	−2	0·55**	0·00	0·07
CCD	0	−0·53**	−0·61**	−0·08
	−1	−0·51**	−0·14	0·10
	−2	−0·02	−0·02	0·67**

[a]Single and double asterisks indicate significance at the $P<0·05$ and $P<0·01$ levels respectively, assuming no temporal autocorrelation between the variables. They therefore show the relative, not absolute, importance of the different satellite sensor variables. In each comparison $n=12$ and degrees of freedom=10.
[b]MIR=middle infra-red radiance data, LST=land surface temperature, NDVI=normalized difference vegetation index, CCD=cold cloud duration.
[c]The time difference between the correlated satellite sensor and malaria admission data: −1 indicates malaria data correlated with satellite data one month previously, etc.

areas. If any of the selected pixels was masked as sea or inland water they were excluded from the calculations. This resulted in a single pixel overlap in the arrays used to calculate the information for Kilifi North and Kilifi South. These values were then transferred to a database and statistical associations explored using the Statistical Package for the Social Sciences (SPSS) version 7.5.1.

Linear regressions were performed to compare the mean monthly percentage of total annual malaria admissions with corresponding monthly Fourier-processed NDVI, LST, MIR and CCD values for each site. Threshold values were then derived from these linear regressions and used to determine the number of months with conditions above these thresholds and therefore likely to be associated with the presentation of clinical malaria in each pixel of the Fourier-processed images of Kenya. The number of months in which clinical malaria could be supported (range 0–12 for each pixel) was then aggregated into zones for comparison with the only other malaria transmission map for Kenya, developed during the colonial era and based on expert opinion of the length of malaria transmission seasons (BUTLER, 1959; see Fig. 4, D). The 1959 map divided the country into zones of malaria transmission periods of less than 3 months, 3–6 months, and over 6 months per year, with large areas classified as 'malarious near water' or 'malaria free'.

Results

Time series data and regression analyses

The different seasonal patterns of malaria admissions recorded are shown in Fig. 1. In Kilifi North (Fig. 1, A) there was a bimodal pattern in annual malaria cases with peaks in admissions around January and July following the short and long rainy seasons respectively. In Kilifi South there was a similar pattern, but it was less pronounced (Fig. 1, B). In contrast, cases of malaria in Siaya (Fig. 1, C) were recorded relatively evenly throughout the year.

The annual time series of the remotely sensed variables (MIR, LST, NDVI and CCD) were derived for each site and compared with the monthly malaria admission data. The general pattern observed at each site was for the peak in vegetation activity to occur approximately one month after the rains, and for it to take a further month for the peak in malaria admissions to become evident. The coefficient of determination (adjusted r^2) resulting from the linear regression of the mean monthly MIR, LST, NDVI and CCD variables against the mean monthly percentage of annual malaria admissions (including lagging the malaria admissions data against the satellite sensor data by one (−1) and two (−2) months) are shown in Table 2. Despite temporal autocorrelation existing between monthly recordings, the coefficient of determination was used to test the relative goodness of fit between malaria admissions and the 4 satellite sensor variables. The strongest correlations were found between malaria admissions and NDVI–1 (mean $r^2=0·71$) and these regressions are shown graphically in Fig. 2. The MIR–1 (mean $r^2=-0·38$) and LST–1 (mean $r^2=-0·33$) variables had inverse relationships with malaria admissions and less significant correlations than with NDVI–1 (Table 2). The negative pattern occurred because the environment tends to be cooler after the rains, due to greater evapo-transpiration from the increasing vegetation cover. There was no evidence that LST limited the potential for clinical malaria at any of the sites monitored. No consistent relationship was found between malaria presentations and CCD. In Siaya the correlation between malaria admissions and CCD–2 was highly significant, but in Kilifi North and South it was very poor (Table 2). Further investigation of the regression plot for Kilifi South (Fig. 3, B) showed a strong linear relationship between malaria presentations and rainfall from February (month 2) until June (month 6), which corresponded with the onset of the long rainy season, but a poor relationship for the rest of the year. This could be explained by the fact that the short rainy season (September–October) maintained suitable conditions for malaria transmission after a history of heavy rainfall. Furthermore, the hydrology in Kilifi South would serve to exacerbate this trend. There was no clear relationship for Kilifi North (Fig. 3, A). Due to the bimodal pattern of annual rainfall on the Kenyan coast complicating the observed relationships with rainfall, and the fact that the MIR and LST variables were never limiting at the sites monitored, the NDVI was selected as the most robust predictor of changes in malaria admission rates because of its highly significant and consistent linear relationship across the 3 study communities.

NDVI thresholds to support clinical malaria

Fig. 2 suggests that a minimum NDVI threshold of between 0·3 and 0·4 is necessary to support any significant seasonal rise in malaria admissions (i.e., by more than 5% of the annual admissions in a given month) at each of the 3 sites. Thresholds of 0·30, 0·35 and 0·40

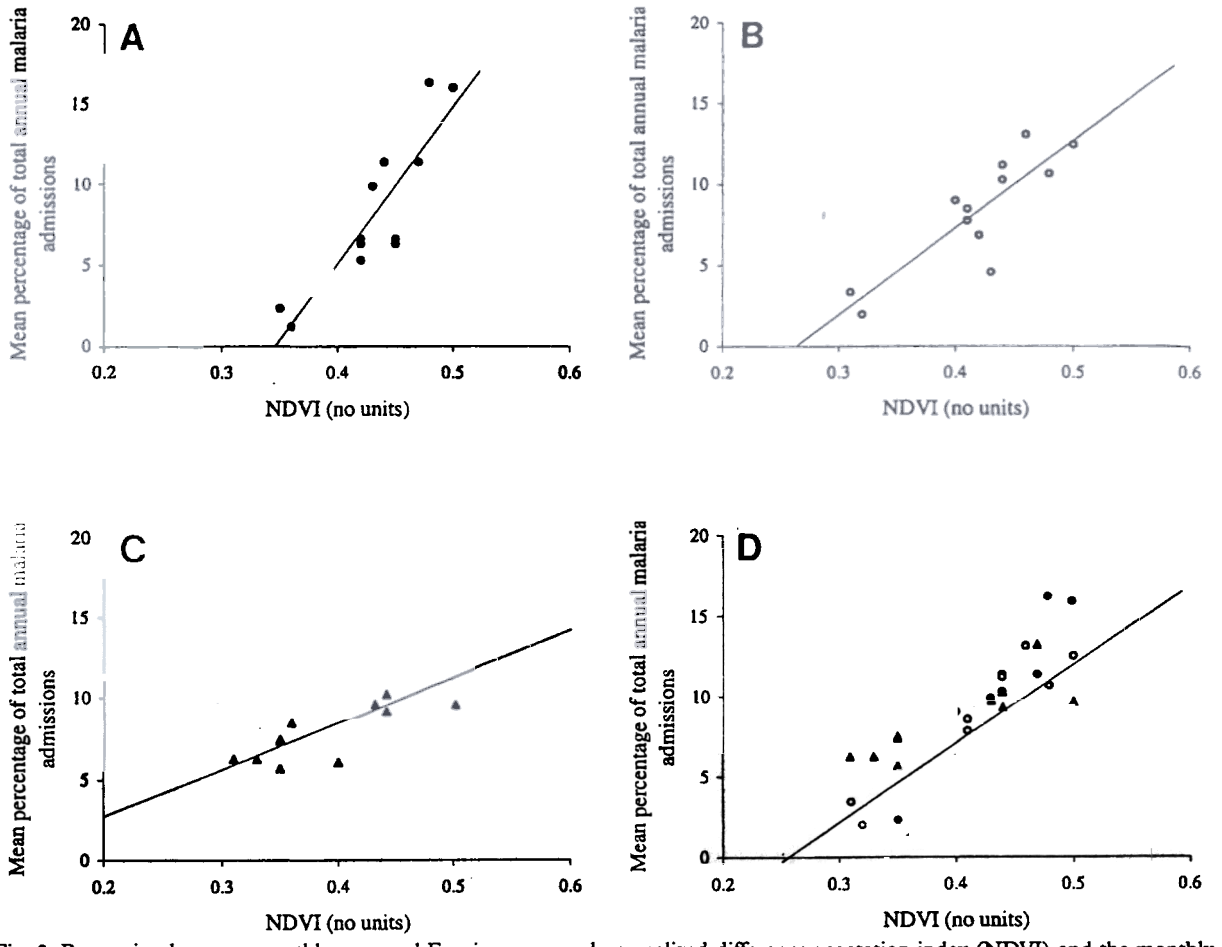

Fig. 2. Regression between monthly temporal Fourier-processed normalized difference vegetation index (NDVI) and the monthly mean percentage of total annual malaria admissions. The NDVI data are lagged by one month. A: Kilifi North (adjusted r^2=0·79, n=12, P<<0·01); B: Kilifi South (r^2=0·74, n=12, P<<0·01); C: Siaya (r^2=0·61, n=12, P<<0·01); D: all 3 sites combined (r^2=0·73, n=36, P<<0·01). (See Table 2 for notes on levels of significance.)

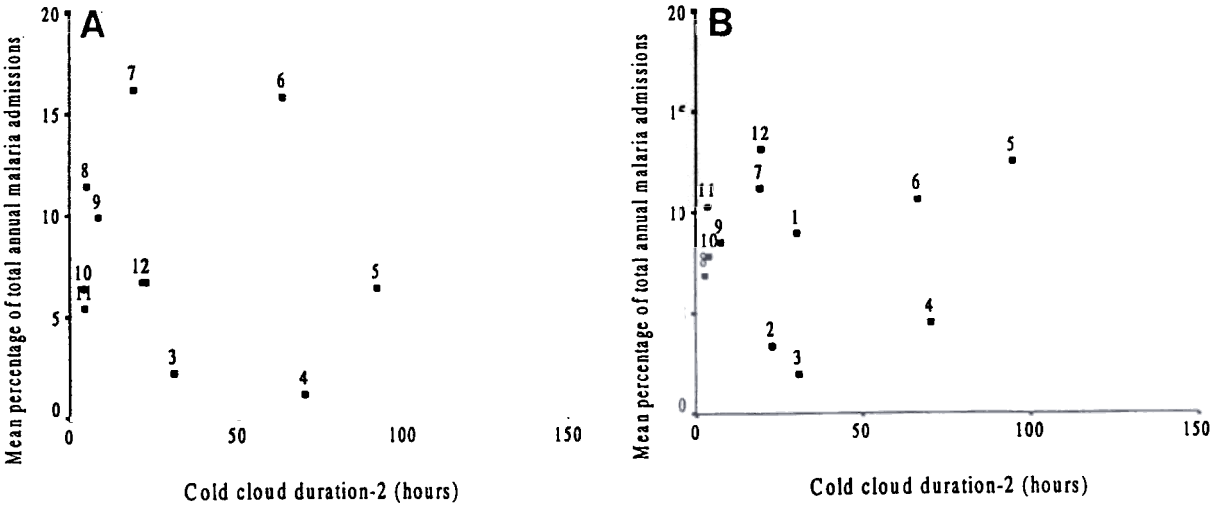

Fig. 3. Regression between monthly temporal Fourier-processed cold cloud duration (CCD) and the monthly mean percentage of total annual malaria admissions. The CCD data are lagged by 2 months (and therefore shown as –2). The months for the malaria records are indicated by numerals adjacent to the points (1 = January, etc.) A: Kilifi North (adjusted r^2 = –0·02, n=12, not significant); B: Kilifi South (r^2 = –0·02, n = 12, not significant). (See Table 2 for notes on levels of significance.)

were therefore applied to the fitted Fourier NDVI time series for Kenya to define the numbers of months in which NDVI exceeded these thresholds and therefore provided conditions suitable for clinical malaria. The results are shown in Fig. 4, B-C for NDVI thresholds of 0·35 and 0·40, respectively; the maps change substantially over this very small NDVI range. In order to compare these patterns of seasonality based upon empirical observations of clinical disease objectively with previous expert opinion of transmission seasons, the monthly

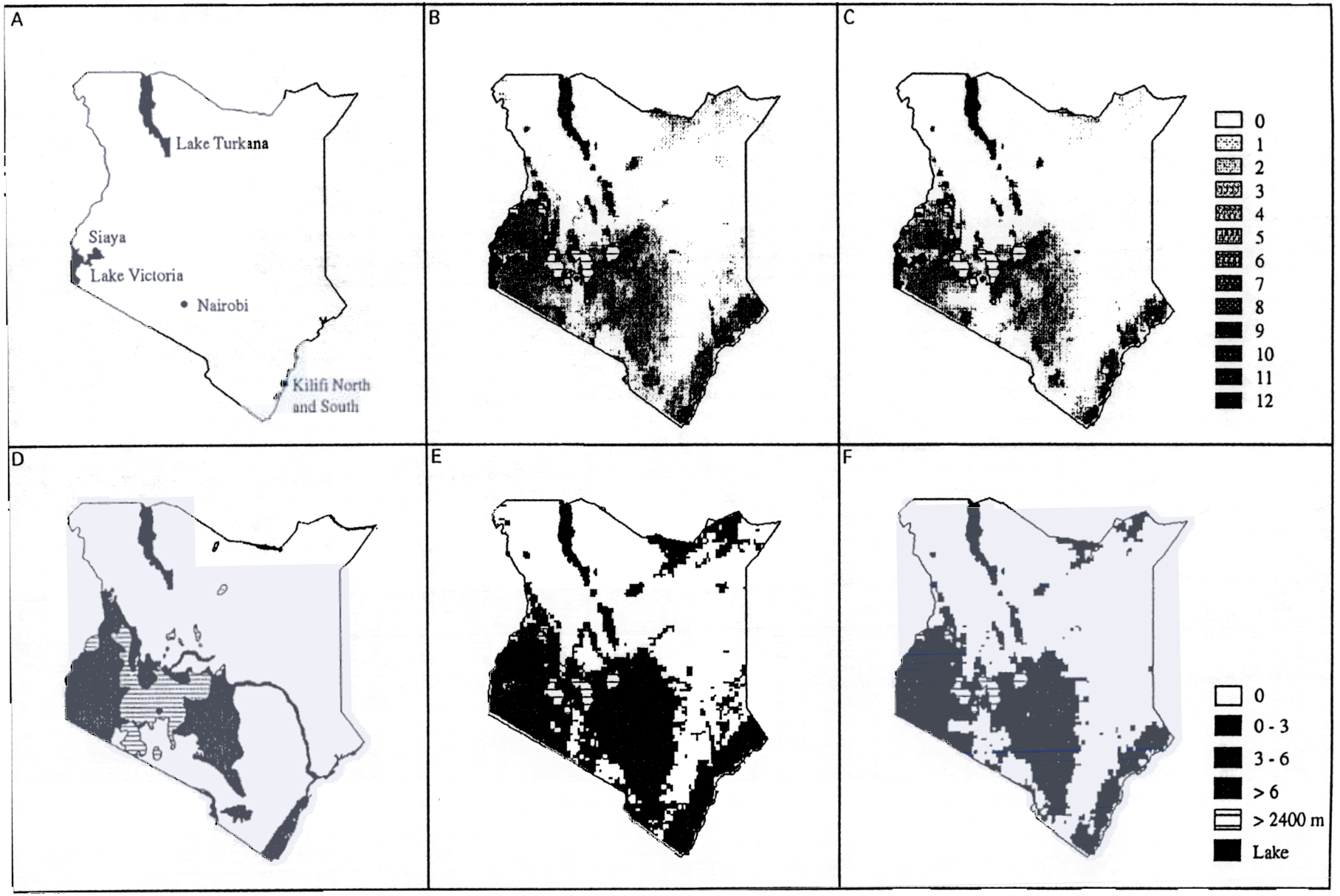

Fig. 4. Maps of predicted malaria seasonality in Kenya. Map A shows the location of the study sites and principle landmarks in Kenya. Maps B and C show the number of months for which malaria transmission is possible, determined by the 0·35 and 0·40 normalized difference vegetation index (NDVI) threshold respectively. Map D is a reproduction of BUTLER's (1959) map of malaria transmission periods in Kenya (the hatched section of this map is simply defined as malaria free and does not relate to the hatched areas above 2400 m in the predicted map; the white area is defined as malarious near water). Maps E and F again show the number of months for which malaria transmission is possible, determined by the 0·35 and 0·40 NDVI threshold respectively but recoded into BUTLER's 1959) categories for visual comparison with D. The keys to the first and second rows of maps are provided on the right of the Figure. North is at the top of each map.

data were recombined according to the definitions used by BUTLER (1959) in preparing the map of malaria transmission in Kenya (Fig. 4, D) using threshold criteria of 0·35 (Fig. 4, E) and 0·40 (Fig. 4, F). Areas above 2400 m were masked in these figures using a digital elevation model (DEM)* because previous investigations in Kenya have found a temperature-dependent absence of transmission above that altitude (GARNHAM, 1948). There is considerable visual correspondence between the predicted maps of malaria transmission periods (Fig. 4, E, F) and expert opinion (Fig. 4, D). The main malaria areas surrounding the central highlands are well defined in kind and extent, as well as variations along the Kenyan coast and the Ethiopian border in the extreme north-east. The malaria seasonality map based on the 0·4 NDVI threshold is the most accurate approximation to BUTLER'S (1959) map.

Discussion

Most clinical staff working in malaria endemic areas of Africa recognize 'malaria seasons' and expert opinion on duration of annual transmission has historically been used to develop malaria maps. There are, however, few examples of empirically developed maps of malaria seasonality related to the clinical outcomes of infection. Programme managers have few resources and thus need to rationalize the control options at their disposal. Annual or biannual treatment of bed nets with insecticides can make a large financial difference to bed net programme budgets. Furthermore, with the rapid emergence of parasite resistance to pyrimethamine/sulfadoxine, the last affordable front-line antimalarial treatment in many countries, restricted use for fever treatment to periods of known disease risk should prolong this drug's useful life span. Targeted chemoprophylaxis has been shown to have a dramatic effect upon child survival (GREENWOOD *et al.*, 1988) and, whilst this intervention is demanding upon resources, logistics, costs and compliance, it is more likely to be acceptable to programme managers and communities when it need be applied for only a few months each year. Moreover, there is renewed interest in the epidemiological features of clinical malaria with the diverse patterns of *P. falciparum* transmission seen in Africa (SNOW *et al.*, 1997; THOMSON *et al.*, 1997). It could be argued that significant proportions of infants born immediately after the acutely seasonal periods of *P. falciparum* challenge will not be actively immunized whilst protected by maternal antibody and other putative innate protective mechanisms, and will thus be at increased risk after their first birthday when first infected in the following season. Furthermore, despite the continued burden malaria places upon child survival in Africa, and many arguments for the utility of disease risk maps, many national malaria control programmes lack this most basic of epidemiological tools.

The application of remote sensing techniques to malaria control has so far been focused on the identification of mosquito habitats and the prediction of mosquito numbers, rather than on the clinical consequences of vector, parasite and human contact. We have studied the characteristically seasonal fluctuations in clinical malaria, in relation to a variety of surrogate meteorological and vegetation variables recorded by sensors on board polar-orbiting and geostationary satellites. The investigation suggests that, whilst changes in LST, MIR and CCD are associated with seasonal changes in the incidence of clinical malaria, they lack sufficient precision and stability across the sites to be of predictive value. Conversely, there was a high and consistent correlation between the temporal changes in the NDVI and the temporal changes in malaria cases across the Kenyan communities studied. There is obviously no direct causal link between NDVI and malaria cases; both factors respond similarly, in direction and magnitude, to changes in meteorological conditions. The NDVI has also been shown to be important in predicting the incidence and prevalence of human trypanosomiasis in Africa (ROGERS, 1991; ROGERS & WILLIAMS, 1993).

The NDVI is potentially, therefore, a very useful predictive tool as it is measured routinely across Africa on a daily basis and is available in the public domain. It would be especially useful if similar relationships between NDVI and malaria admissions were to be identified in other parts of Africa. Recent analyses in The Gambia, however, indicate that different thresholds may apply in the savannah areas of West Africa (THOMSON *et al.*, 1997), so that area-specific modelling may be required. Further complications arise due to the low spatial resolution of the NDVI data. An 8×8 km pixel is a spatial average that is likely to be composed of regions above and below the 0·3–0·4 NDVI threshold, so that in the current analysis small areas suitable for malaria transmission would not be detected. Increasing the utility of such observations to location-specific information on the spatial and temporal patterns of disease will obviously require commensurate increases in the temporal and spatial resolutions of the satellite sensor data.

The maps of seasonal clinical disease developed for Kenya in this investigation were based upon the empirical observation that clinical malaria could be supported only whilst NDVI exceeded a threshold value of between 0·3 and 0·4. The maps shown in Fig. 4, E and F agree with expert opinion of the length of the transmission seasons reported during the late 1950s in excluding the potential transmission of malaria in the arid regions of Kenya (north-eastern provinces and the area inland from the coastal strip). The most sensitive indicator is an NDVI index of 0·4 (Fig. 4, F), which provides a close approximation to the differentials in transmission seasons in western Kenya and along the coast, as suggested by the 1959 transmission map (BUTLER, 1959). It is stressed that the current maps merely demonstrate a method and do not constitute a definitive picture of malaria seasonality in Kenya. To develop this work there is a need to conduct further validation or 'ground-truthing' of the relationships between malaria admissions and environmental data for much wider geographical areas, as well as to explore predictive models of seasonality.

It is perhaps not by coincidence that previous maps of the annual periods of transmission have often been used as empirical maps of intensity of transmission, on the assumption that the longer the period of transmission the greater is the potential for higher host infection rates. Confusion over appropriate definitions of endemicity has hampered the use of epidemiological maps for malaria control (SNOW *et al.*, 1996). Nevertheless, it is notable that those areas where NDVI thresholds for clinical disease are exceeded for 11 to 12 months of the year do support the highest rates of *P. falciparum* infection among the host population in Kenya (OMUMBO *et al.*, in press), indicating the potential of these remotely sensed images for predicting the intensity of transmission, as well as length of malaria seasons.

To conclude, it has been demonstrated that a significant correlation exists between the timing of changes of meteorological and vegetation variables recorded by satellite sensors and the relative changes in prevalence of clinical malaria, and these correlations have been used to produce clinical disease seasonality maps for Kenya. Moreover, satellite systems scheduled for orbit in the near future will carry sensors with spectral, spatial and temporal resolutions far exceeding the specification of those on existing satellite series (see HAY, 1997). For example, the geostationary Meteostat Second Generation (MSG) satellite to be launched in the year 2000 will

*Anonymous (1996). GTOPO30 Documentation. Universal Resource Locator <http://edcwww.cr.usgs.gov/landdac/gtopo30/README.html>. Sioux Falls, South Dakota, USA: EROS Data Center, Global Land Information System.

be able to acquire NDVI images for the whole of Africa, at 1 × 1 km resolution, every 15 min during daylight hours (SCHMETZ *et al.*, 1995). These existing and future information sources, which will be provided freely to African countries, when combined with models of disease transmission intensity and other available demographic, socioeconomic and health service information, could be used to create maps to guide in the selection and timing of interventions. This would provide a more cost-effective and objective basis for malaria control.

Acknowledgements

This study received financial support from the Wellcome Trust and the Medical Research Council, UK, the Centers for Disease Surveillance and National Center for Infectious Diseases, USA, and the Kenyan Medical Research Council. R.W.S. is a Senior Wellcome Trust Fellow in Basic Biomedical Sciences (no. 033340). In addition, this publication is an output from research equipment funded by the Department for International Development (DfID), UK (Livestock Production Programme ZC0012). However, the DfID can accept no responsibility for information provided or views expressed. The following formal acknowledgement is requested of those who use PAL data: 'data used in this study include data produced through funding from the Earth Observing System Pathfinder Program of NASA's Mission to Planet Earth in cooperation with National Oceanic and Atmospheric Administration. The data were provided by the Earth Observing System Data and Information System (EOSDIS), Distributed Active Archive Center (DAAC) at Goddard Space Flight Center which archives, manages and distributes this dataset'. We also thank Dr Kevin Marsh for general support and Drs Byron Wood, Sarah Randolph, Madeleine Thomson, Robert Green, Tim Robinson, Mike Packer and Peter Stevenson, and 2 anonymous referees, for comments on the manuscript. Dr William Wint provided much valued help with Geographic Information System manipulations and in the final preparation of the colour figures. This paper is published with the permission of the director of the Kenya Medical Research Institute.

References

Agbu, P. A. & James, M. E. (1994). *The NOAA/NASA Pathfinder AVHRR land data set user's manual.* Greenbelt, Maryland: Goddard Distributed Active Archive Center.

Anonymous (1994). *Information on meteorological and other environmental satellites*, 3rd edition. Geneva: World Meteorological Organization, publication no. 411.

Beck, L. R., Rodriguez, M. H., Dister, S. W., Rodriguez, A. D., Rejmankova, E., Ulloa, A., Meza, R. A., Roberts, D. R., Paris, J. F., Spanner, M. A., Washino, R. K., Hacker, C. & Legters, L. J. (1994). Remote sensing as a landscape epidemiologic tool to identify villages at high risk for malaria transmission. *American Journal of Tropical Medicine and Hygiene*, **51**, 271–280.

Beck, L. R., Rodriguez, M. H., Dister, S. W., Rodriguez, A. D., Washino, R. K., Roberts, D. R. & Spanner, M. A. (1997). Assessment of a remote sensing-based model for predicting malaria transmission risk in villages of Chiapas, Mexico. *American Journal of Tropical Medicine and Hygiene*, **56**, 99–106.

Binka, F. N., Morris, S. S., Ross, D. A., Arthur, P. & Aryeetey, M. R. (1994). Patterns of malaria morbidity and mortality in children in northern Ghana. *Transactions of the Royal Society of Tropical Medicine and Hygiene*, **88**, 381–385.

Bouvier, P., Breslow, N., Ogobara, D., Robert, C. F., Picquet, M., Mauris, A., Dolo, A., Dembele, H. K., Delley, V. & Rougemont, A. (1997). Seasonality, malaria and impact of prophylaxis in a West African village. II: Effect on birth weight. *American Journal of Tropical Medicine and Hygiene*, **56**, 384–389.

Boyd, D. S. & Curran, P. J. (in press). Using remote sensing to reduce uncertainties in the global carbon budget: the potential of radiation acquired in the middle infrared wavelengths. *Remote Sensing Reviews.*

Boyd, D. S., Foody, G. M., Curran, P. J., Lucas, R. M. & Honzak, M. (1996). An assessment of radiance in Landsat TM middle and thermal infrared wavebands for the detection of tropical forest regeneraiton. *International Journal of Remote Sensing*, **17**, 249–261.

Brewster, D. R. & Greenwood, B. M. (1993). Seasonal variation of paediatric diseases in The Gambia, West Africa. *Annals of Tropical Paediatrics*, **13**, 133–146.

Butler, R. J. (1959). *Atlas of Kenya: a comprehensive series of new and authenticated maps prepared from the national survey and other governmental sources with gazetteer and notes on pronunciation and spelling*, 1st edition. Nairobi: The Survey of Kenya.

Cooper, D. R. & Asrar, G. (1989). Evaluating atmospheric correction models for retrieving surface temperatures from the AVHRR over a tallgrass prairie. *Remote Sensing of Enviroment*, **27**, 93–102.

Cracknell, A. P. (1997). *The Advanced Very High Resolution Radiometer.* London: Taylor & Francis.

Dietz, K. (1988). Mathematical models for transmission and control of malaria. In: *Malaria: Principles and Practice of Malariology*, volume 2, Wernsdorfer, W. H. & McGregor, I. (editors). London: Churchill Livingstone, pp. 1091–1133.

Dugdale, G., McDougall, V. & Thorne, V. (1995). The TAMSAT method for estimating rainfall over Africa and its implications. In: *RSS95: Remote Sensing in Action. Proceedings of the 21st Annual Conference of the Remote Sensing Society.* Nottingham: The Remote Sensing Society, pp. 773–780.

Garnham, P. C. C. (1948). The incidence of malaria at high altitudes. *Journal of the National Malaria Society*, **7**, 275–284.

Gazin, P., Robert, V., Cot, M., Simon, J., Halna, J. M., Darriet, F., Legrand, D., Carnevale, P. & Ambroise-Thomas, P. (1988). Le paludisme dans l'Oudalan, région Sahelienne du Burkina Faso. *Annales de la Société Belge de Médecine Tropicale*, **68**, 255–264.

Greenwood, B. M. & Pickering, H. (1993). A malaria control trial using insecticide-treated bed nets and targeted chemoprophylaxis in a rural area of The Gambia, West Africa. A review of the epidemiology and control of malaria in The Gambia, West Africa. *Transactions of the Royal Society of Tropical Medicine and Hygiene*, **87**, supplement 2, S3–S11.

Greenwood, B. M., Bradley, A. K., Greenwood, A. M., Byass, P., Jammeh, K., Marsh, K., Tullock, S., Oldfield, F. J. S. & Hayes, R. (1987). Mortality and morbidity from malaria among children in a rural area of The Gambia, West Africa. *Transactions of the Royal Society of Tropical Medicine and Hygiene*, **81**, 478–486.

Greenwood, B. M., Bradley, A. K., Byass, P., Greenwood, A. M., Snow, R. W., Hayes, R. J. & N'Jie, A. B. H. (1988). Comparison of two strategies for control of malaria within a primary health care programme in The Gambia. *Lancet*, **i**, 1121–1127.

Hay, S. I. (1996). *An investigation of the utility of remotely sensed meteorological satellite data for predicting the distribution and abundance of the tsetse fly (Diptera: Glossinidae).* University of Oxford, DPhil thesis.

Hay, S. I. (1997). Remote sensing and disease control: past, present and future. *Transactions of the Royal Society of Tropical Medicine and Hygiene*, **91**, 105–106.

Hay, S. I., Tucker, C. J., Rogers, D. J. & Packer, M. J. (1996). Remotely sensed surrogates of meteorological data for the study of the distribution and abundance of arthropod vectors of disease. *Annals of Tropical Medicine and Parasitology*, **90**, 1–19.

Hay, S. I., Packer, M. J. & Rogers, D. J. (1997). The impact of remote sensing on the study and control of invertebrate intermediate hosts and vectors for disease. *International Journal of Remote Sensing*, **18**, 2899–2930.

Holben, B. N. (1986). Characteristics of maximum value composite images from temporal AVHRR data. *International Journal of Remote Sensing*, **7**, 1417–1434.

James, M. E. & Kalluri, S. N. V. (1994). The pathfinder AVHRR land data set—an improved coarse resolution data set for terrestrial monitoring. *International Journal of Remote Sensing*, **15**, 3347–3363.

Justice, C. O., Townshend, J. R. G., Holben, B. N. & Tucker, C. J. (1985). Analysis of the phenology of global vegetation using meteorological satellite data. *International Journal of Remote Sensing*, **6**, 1271–1318.

Kerber, A. G. & Schutt, J. B. (1986). Utility of AVHRR channel 3 and 4 in land-cover mapping. *Photogrammetric Engineering and Remote Sensing*, **52**, 1877–1883.

Kidwell, K. B. (1995). *NOAA polar orbiter data users' guide (TIROS-N, NOAA-6, NOAA-7, NOAA-8, NOAA-9, NOAA-10, NOAA-11, NOAA-12, NOAA-13 and NOAA-14).* Washington, DC: National Oceanic and Atmospheric Administration.

Lambin, E. F. & Ehrlich, D. (1995). Combining vegetation indexes and surface temperature for land-cover mapping at broad spatial scales. *International Journal of Remote Sensing*, **16**, 573–579.

Linthicum, K. J., Bailey, C. L., Glyn Davies, F. & Tucker, C. J. (1987). Detection of Rift Valley fever viral activity in Kenya by satellite remote sensing imagery. *Science*, **235**, 1656–1659.

Muir, D. A. (1988). Anopheline mosquitoes: vector reproduc-

tion, life-cycle and biotype. In: *Malaria: Principles and Practice of Malariology*, volume 2, Wernsdorfer, W. H. & McGregor, I. (editors). London: Churchill Livingstone, pp. 431–451.

Omumbo, J., Ouma, J., Rapouda, B., Craig, M. H., Le Sueur, D. & Snow, R. W. (in press). Mapping malaria transmission intensity using geographical information systems (GIS): an example from Kenya. *Annals of Tropical Medicine and Parasitology.*

Myneni, R. B., Maggion, S., Iaquinto, J., Privette, J. L., Gobron, N., Pinty, B., Kimes, D. S., Verstraete, M. M. & Williams, D. L. (1995). Optical remote sensing of vegetation: modeling, caveats, and algorithms. *Remote Sensing of Environment*, **51**, 169–188.

Pope, K. O., Rejmankova, E., Savage, H. M., Arredondo-Jimenez, J. I., Rodriguez, M. H. & Roberts, D. R. (1994). Remote sensing of tropical wetlands for malaria control in Chiapas, Mexico. *Ecological Applications*, **4**, 81–90.

Price, J. C. (1984). Land surface temperature measurements from the split window channels of the NOAA 7 advanced very high resolution radiometer. *Journal of Geophysical Research*, **89**, 7231–7237.

Rejmankova, E., Roberts, D. R., Pawley, A., Manguin, S. & Polanco, J. (1995). Predictions of adult *Anopheles albimanus* densities in villages based on distances to remotely sensed larval habitats. *American Journal of Tropical Medicine and Hygiene*, **53**, 482–488.

Roberts, D. R., Paris, J. F., Manguin, S., Harbach, R. E., Woodruff, R., Rejmankova, E., Polanco, J., Wullschleger, B. & Legters, L. J. (1996). Predictions of malaria vector distribution in Belize based on multispectral satellite data. *American Journal of Tropical Medicine and Hygiene*, **54**, 304–308.

Rogers, D. J. (1991). Satellite imagery, tsetse and trypanosomiasis in Africa. *Preventive Veterinary Medicine*, **11**, 201–220.

Rogers, D. J. & Williams, B. G. (1993). Monitoring trypanosomiasis in space and time. *Parasitology*, **106**, S77–S92.

Rogers, D. J. & Williams, B. G. (1994). Tsetse distribution in Africa: seeing the wood and the trees. In: *Large-scale Ecology and Conservation Biology*, Edwards, P. J., May, R. M. & Webb, N. R. (editors). Oxford: Blackwell Scientific Publications, pp. 249–273.

Rogers, D. J., Hay, S. I. & Packer, M. J. (1996). Predicting the distribution of tsetse flies in West Africa using temporal Fourier processed meteorological satellite data. *Annals of Tropical Medicine and Parasitology*, **90**, 225–241.

Schmetz, J., Klaes, D. & Rattenborg, M. (1995). Meteorological products from current and future EUMETSAT satellite systems. In: *Proceedings of the 1995 Meteorological Satellite Data Users' Conference*. Darmstadt: EUMETSAT, publication no. EUM P 17, pp. 233–240.

Sellers, P. J. (1985). Canopy reflectance, photosynthesis and transpiration. *International Journal of Remote Sensing*, **6**, 1335–1372.

Slutsker, L., Taylor, T. E., Wirima, J. J. & Steketee, R. W. (1994). In-hospital morbidity and mortality due to malaria-associated severe anaemia in two areas of Malawi with different patterns of malaria infection. *Transactions of the Royal Society of Tropical Medicine and Hygiene*, **88**, 548–551.

Smith, T., Charlwood, J. D., Kihonda, J., Mwankuyse, S., Billingsley, P., Meuwissen, J., Lyimo, E., Takken, W., Teuscher, T. & Tanner, M. (1993). Absence of seasonal variation in malaria parasitaemia in an area of intense seasonal transmission. *Acta Tropica*, **54**, 55–72.

Snijders, F. L. (1991). Rainfall monitoring based on Meteosat data — a comparison of techniques applied to the western Sahel. *International Journal of Remote Sensing*, **12**, 1331–1347.

Snow, R. W., Armstrong-Schellenberg, J. R. M., Peshu, N., Forster, D., Newton, C. R. J. C., Winstanley, P. A., Mwangi, I., Waruiru, C., Warn, P. A., Newbold, C. & Marsh, K. (1993). Periodicity and space–time clustering of severe childhood malaria on the coast of Kenya. *Transactions of the Royal Society of Tropical Medicine and Hygiene*, **87**, 386–390.

Snow, R. W., Marsh, K. & le Sueur, D. (1996). The need for maps of transmission intensity to guide malaria control in Africa. *Parasitology Today*, **12**, 455–457.

Snow, R. W., Omumbo, J. A., Lowe, B., Molyneux, S. M., Obiero, J. O., Palmer, A., Weber, M. W., Pinder, M., Nahlen, B., Obonyo, C., Newbold, C., Gupta, S. & Marsh, K. (1997). Relation between severe malaria morbidity in children and level of *Plasmodium falciparum* transmission in Africa. *Lancet*, **349**, 1650–1654.

Stowe, L. L., McClain, E. P., Carey, R., Pellegrino, P., Gutman, G. G., Davia, P., Long, C. & Hart, S. (1991). Global distribution of cloud cover derived from NOAA/AVHRR operational satellite data. *Advances in Space Research*, **11**, 51–54.

Sugita, M. & Brutasaert, W. (1993). Comparison of land surface temperatures derived from satellite observations with ground truth during FIFE. *International Journal of Remote Sensing*, **14**, 1659–1676.

Thomson, M. C., Connor, S. J., Milligan, P. J. M. & Flasse, S. P. (1996). The ecology of malaria — as seen from Earth observation satellites. *Annals of Tropical Medicine and Parasitology*, **90**, 243–264.

Thomson, M. C., Connor, S. J., Milligan, P. & Flasse, S. P. (1997). Mapping malaria risk in Africa: what can satellite data contribute? *Parasitology Today*, **13**, 313–318.

Tucker, C. J. (1979). Red and photographic infrared linear combinations for monitoring vegetation. *Remote Sensing of Environment*, **8**, 127–150.

Tucker, C. J. & Sellers, P. J. (1986). Satellite remote sensing of primary production. *International Journal of Remote Sensing*, **7**, 1395–1416.

Tucker, C. J., Townshend, J. R. G. & Goff, T. E. (1985a). African land-cover classification using satellite data. *Science*, **227**, 369–375.

Tucker, C. J., Vanpraet, C. L., Sharman, M. J. & Van Ittersum, G. (1985b). Satellite remote sensing of total herbaceous biomass production in the Senegalese Sahel: 1980–1984. *Remote Sensing of Environment*, **17**, 233–249.

Wagner, V. E., Hill-Rowley, R., Narlock, S. A. & Newson, H. D. (1979). Remote sensing: a rapid and accurate method of data acquisition for a newly formed mosquito control district. *Mosquito News*, **39**, 283–287.

Wood, B. L., Beck, L. R., Washino, R. K., Hibbard, K. A. & Salute, J. S. (1992). Estimating high mosquito-producing rice fields using spectral and spatial data. *International Journal of Remote Sensing*, **13**, 2813–2826.

Received 11 September 1997; revised 14 October 1997; accepted for publication 5 November 1997